ACS APPLIED ENERGY MATERIALS

www.acsaem.org Article

# Atomic Layer Deposition of $SnO_2$ as an Electron Transport Material for Solid-State P-type Dye-Sensitized Solar Cells

Haoliang Cheng, Yawen Liu, Bin Cai, Carl Hägglund, Tomas Kubart, Gerrit Boschloo, and Haining Tian*

Cite This: *ACS Appl. Energy Mater.* 2022, 5, 12022−12028 Read Online

ACCESS | Metrics & More | Article Recommendations | Supporting Information

**ABSTRACT:** Tin oxide ($SnO_2$) as an electron transport material was prepared by atomic layer deposition in dye-sensitized NiO films to fabricate solid-state p-type dye-sensitized solar cells using two organic dyes PB6 and TIP as photosensitizers. Due to the excellent electron mobility and satisfactory penetration of $SnO_2$ material into the NiO film, a record photocurrent density over 1 mA $cm^{-2}$ was achieved with a power conversion efficiency of 0.14%. The effect of an inserted $Al_2O_3$ layer between the dye-sensitized NiO and $SnO_2$ layer on photovoltaic performance of the devices was also investigated. The results suggest that the charge recombination between NiO and $SnO_2$ can be significantly suppressed, showing prolonged charge lifetime and enhanced photovoltage.

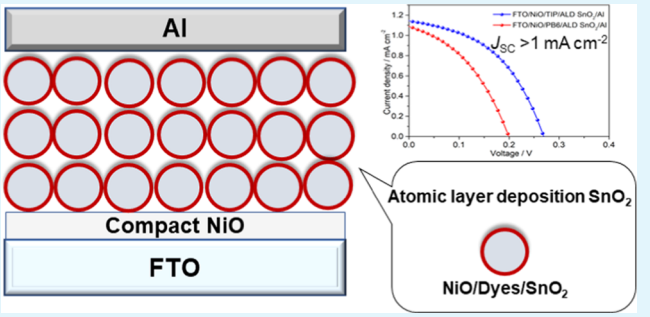


**KEYWORDS:** *atomic layer deposition, electron transport materials, high current density, p-type DSSCs, tin oxide*



## INTRODUCTION

Since the report of pioneer work by O'Regan and Grätzel and co-authors in 1991,[1] dye-sensitized solar cells (DSSCs) have attracted great attention.[2] The traditional DSSCs, also called n-type DSSCs, are based on dye-sensitized $TiO_2$ photoanodes, which have experienced rapid progress during the past three decades.[3,4] In 1999, Lindquist and co-authors reported p-type DSSCs with a liquid electrolyte in which dye-sensitized NiO films were used as a photocathode.[5] The photocathode plays a vital role in tandem DSSCs, which could reach a theoretical power conversion efficiency (PCE) of more than 30%. However, the development of p-type DSSCs is still far behind that of n-type DSSCs.[6] Various studies have been focused on improving the performance of p-type DSSCs[7−11] because of their good potential in tandem solar cells and solar fuel devices.[12,13]

The traditional liquid p-type DSSCs consist of a dye-sensitized mesoporous NiO photocathode, an $I^-/I_3^-$ redox couple, and a counter electrode. Due to the small energy difference between the valence band (VB) of NiO and reduction potential of $I^-/I_3^-$, the open-circuit voltage ($V_{oc}$) of p-type DSSCs is normally very low, less than 200 mV.[14,15] In addition, the severe charge recombination in liquid p-type DSSCs also leads to the low $V_{oc}$ and poor fill factor (FF).[16,17] Moreover, the stability of the liquid device due to potential electrolyte leaking is always a concern. Besides the good stability, the solid-state p-type DSSCs can achieve high voltage because of high energy difference between the VB of NiO and the conduction band (CB) of electron transport material (ETM). In 2014, our group[18] reported the first example of solid-state p-type DSSCs using P1 dye as a photosensitizer and PCBM as ETM, which achieved a $V_{oc}$ of 620 mV. A slow charge recombination between holes in NiO and electrons in $PCBM^-$ was observed. However, the photocurrent density ($J_{sc}$, 50 $\mu$A $cm^{-2}$) of such a device was extremely low because of the low electron mobility and thick layer of PCBM. Other diketopyrrolopyrrole derivatives have also been used in the PCBM-based solid-state p-type DSSCs, showing an enhanced $J_{sc}$ of 0.45 mA $cm^{-2}$ because of their strongly reducing ability and long lifetime of the charge-separated state.[19] Subsequently, our group employed inorganic metal oxides ($TiO_2$ and ZnO) with high electron mobility as ETM.[20−23] Atomic layer deposition (ALD) of $TiO_2$ has been proved to be able to enhance ultrafast charge separation and dye regeneration ($t_{1/2} \leq 500$ fs) in a core−shell NiO-dye−$TiO_2$ film.[21] Although the photocurrent density of the solar cell using ZnO as ETM has made a big improvement,[23] the $J_{sc}$ of solid-state p-type DSSCs was still lower than 1 mA $cm^{-2}$, which was much lower than that of liquid p-type DSSCs. According to our previous study,

**Received:** May 2, 2022
**Accepted:** September 13, 2022
**Published:** September 26, 2022

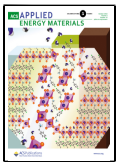

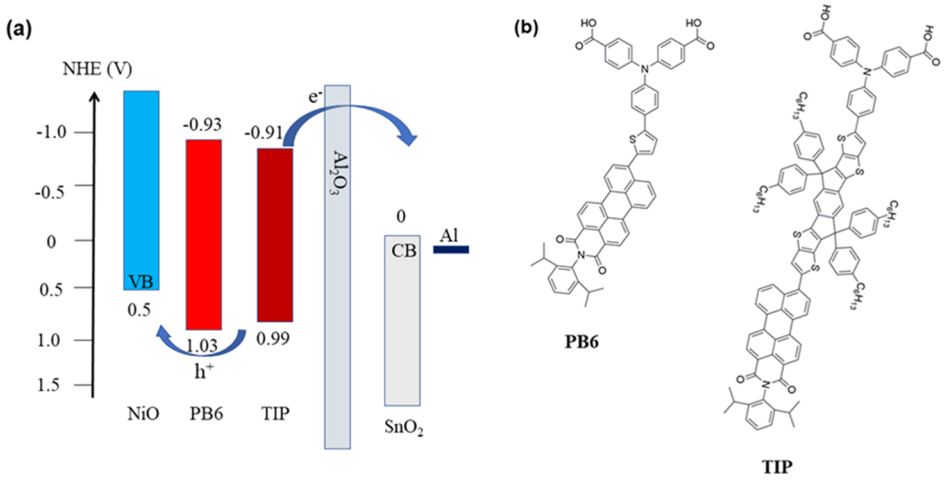


**Figure 1.** (a) Energy levels of components used in p-type solid-state DSSCs with ALD $SnO_2$ as ETM. (b) Molecular structures of PB6 and TIP dyes.

the fact that a majority of dyes are not entirely electrically connected with the ETM contributes to the low $J_{sc}$ of solid-state p-type DSSCs.[24] These results encouraged us to further explore other suitable metal oxides as ETMs and improve photovoltaic parameters.[25]

Tin oxide ($SnO_2$) is an n-type metal oxide semiconductor with high electron mobility and stability, which has been used as ETM in perovskite solar cells.[26,27] Its electron mobility can reach as high as 410 $cm^2\ V^{-1}\ s^{-1}$.[28] In this work, we employed $SnO_2$ as ETM in solid-state p-type DSSCs. To make good penetration of $SnO_2$ into dye-sensitized NiO films, the ALD method was employed. By extending the exposure and purge time in the process of ALD of $SnO_2$, good contact between dye-sensitized mesoporous NiO films and $SnO_2$ can be achieved, which is helpful for efficiently extracting electrons from the dyes after hole injection into NiO. A record $J_{sc}$ over 1 mA $cm^{-2}$ was reached for solid-state p-type DSSCs. In addition, introduction of ALD $Al_2O_3$ between the dye-sensitized NiO and $SnO_2$ layer can suppress the charge recombination, resulting in an obvious enhancement of the photovoltage.

## EXPERIMENTAL SECTION

**Materials.** PB6[21] and TIP[23] dyes were reported in our previous work. Fluorine-doped tin-oxide coated glass (FTO, TEC15) was purchased from Pilkington. *tert*-Butanol, acetonitrile, zinc powder, and hydrochloric were purchased from Sigma-Aldrich. Aluminum (Al) wire was purchased from Umicore.

**Device Fabrication.** The FTO conductive glass substrates were etched with 2 M hydrochloric and zinc powder. The etched FTO substrates were washed with detergents, deionized water, acetone, and ethanol using an ultrasonic bath. Then, the cleaned FTO were dried with flow $N_2$. A compact NiO blocking layer (80 nm) was deposited on the FTO substrate by reactive magnetron sputtering. The deposition condition is the same as our previous work.[21] Before screen printing the mesoporous NiO film, the sputtered NiO blocking layer was annealed in an oven at 450 °C for 0.5 h in an ambient atmosphere. The NiO paste was prepared according to the previous literature.[22] Then, one layer of mesoporous NiO films with a thickness of 750 nm was deposited on the blocking layer by the screen printing method. The screen-printed NiO film was transferred into an oven and sintered at 450 °C for 30 min. After cooling to room temperature, the mesoporous NiO films were dipped into a 0.2 mM dye (PB6 or TIP) *tert*-butanol/acetonitrile (v/v = 1:1) solution for 16 h. Subsequently, the sensitized NiO film was rinsed with ethanol and dried with $N_2$ flow. The ETM $SnO_2$ was deposited in the NiO film by the ALD method. The back-contact (Al) electrode was deposited on the ALD $SnO_2$ film with a thickness of 120 nm. For NiO/dye/$Al_2O_3$/$SnO_2$-based devices, the point $Al_2O_3$ was inserted after NiO sensitization but before ALD of $SnO_2$.

**ALD of $Al_2O_3$ and $SnO_2$.** The ALD employed a stop-flow process in the project. The precursors for ALD of $Al_2O_3$ were composed of trimethylaluminum (TMA) and deionized water ($H_2O$). The temperature of the chamber was 120 °C with a stability time of 1 h before the ALD process. In total, 10 cycles of $Al_2O_3$ were deposited on the NiO film.

The stop flow involved a sequence of (1) reduced carrier gas flow, (2) reduced pumping speed through a bypass constriction, (3) precursor injection, (4) precursor exposure, (5) restored pumping speed, and (6) restored carrier gas flow and purging. For the TMA precursor, the duration of steps 1 to 6 were 2, 2, 0.2, 21.8, 2, and 2 s. During this sequence, the carrier gas flow was reduced from 40 to 10 standard cubic centimeters per minute (sccm) in each of the five unused precursor lines of the system. The TMA line used a flow of 150 sccm during the injection step. In the $H_2O$ half-cycle, the duration of steps 1 to 6 was the same, that is, 2, 2, 0.2, 21.8, 2, and 2 s, while the $H_2O$ carrier gas flow was increased to 150 sccm and the other precursor line flows were reduced to 10 sccm.

The precursor of ALD $SnO_2$ was composed of tetrakis-(dimethylamido)tin (TDMASn) and deionized water ($H_2O$) and used the same stop-flow time sequence as for the $Al_2O_3$ ALD. The carrier gas ($N_2$) flow was 200 and 200 sccm during the TDMASn and $H_2O$ injection steps, respectively. In all, 100 cycles of $SnO_2$ were deposited on the NiO film. A slide of Si wafers was used to evaluate the thickness of $SnO_2$ and $Al_2O_3$ with a spectroscopic ellipsometer.

**Device Characterization.** The sputtering of NiO films was performed on a Von Ardenne magnetron sputter system (CS730S) with a Ni target. The ALD was performed on a new PICOSUN R-200 advanced ALD system. The back-contact layer (Al) was deposited on a Lesker PVD 75 evaporator. Current density−voltage ($J$−$V$) curves were measured using a Newport solar simulator (model 91160, AM 1.5 G) equipped with a Keithley 2400 source meter. Before measurement, the light intensity (100 mW $cm^{-2}$) was calibrated with a calibrated filter Si cell. The area of the mask was 0.125 $cm^2$ during the measurement. The incident photon-to-current efficiency (IPCE) spectrum was measured with a setup consisting of a xenon lamp (Spectral Products ASB-XE-175), a monochromator (Spectral Products CM110), and a Labjack U6 DAQ board. The IPCE device was calibrated with a Si solar cell before measurement.

**Transient Photocurrent and Photovoltage Measurements.** The transient photocurrent and photovoltage measurements were conducted using a Dyenamo tool-box DN-AE01 system. The light intensity (white LED light, Luxeon Star 1 W) was adjusted by


https://doi.org/10.1021/acsaem.2c01328
ACS Appl. Energy Mater. 2022, 5, 12022−12028

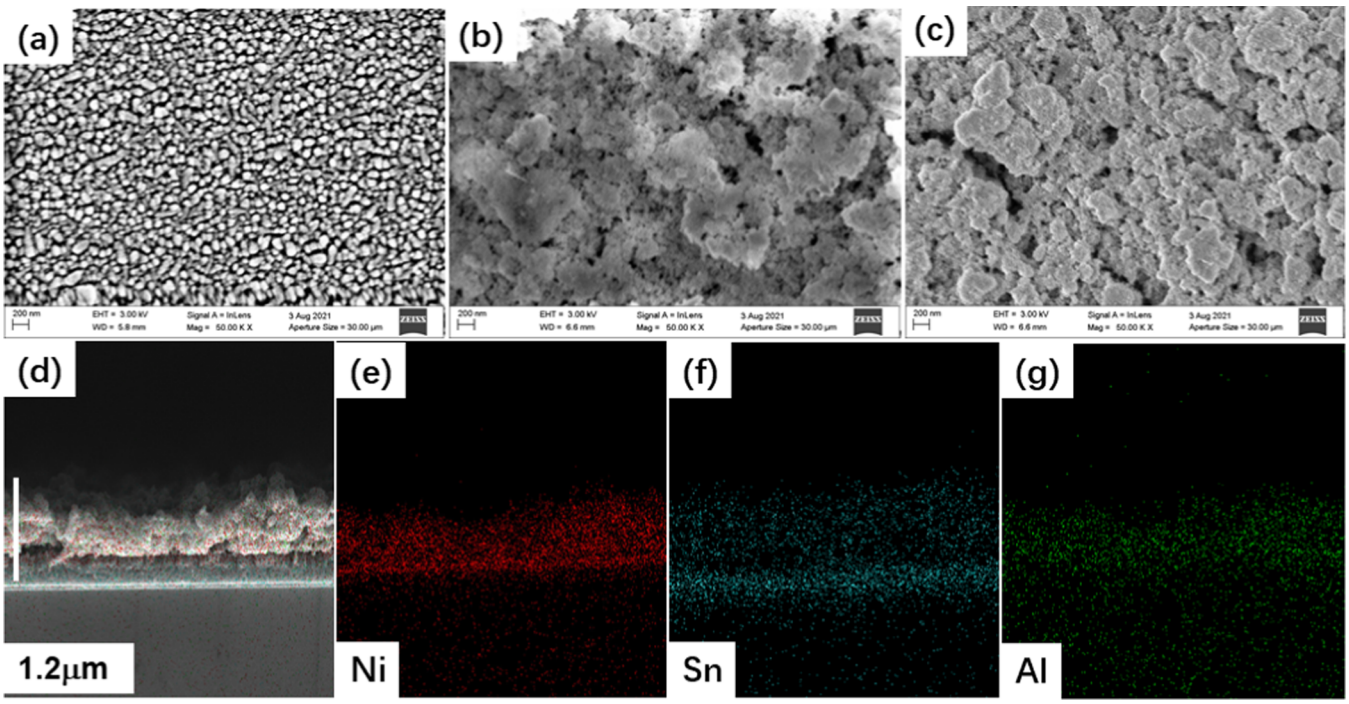


**Figure 2.** (a) SEM image of the sputter-deposited NiO blocking layer on the FTO substrate, (b) SEM image of mesoporous NiO films; (c) SEM image of atomic layer-deposited $SnO_2$ film on the FTO/NiO film; (d) cross-section SEM image of FTO/NiO/PB6/ALD $Al_2O_3$/ALD $SnO_2$; and (e–g) EDX element mapping of Ni, Sn, and Al.

changing the applied voltage. The charge lifetime and charge transport lifetime were achieved by fitting the decay of the transient photocurrent and transient photovoltage, respectively.

## RESULTS AND DISCUSSION

The device structure of the solid-state p-type DSSCs, which is composed of electrodes (FTO/NiO), dyes (PB6 or TIP), ETM (ALD $SnO_2$), and back-contact material (Al), is shown in Figure 1. The energy levels of components used in solid-state p-type DSSCs are illustrated in Figure 1a. Under light illumination, the excited dye injects hole into the NiO VB, and then, the reduced dye injects electron into the $SnO_2$ CB. Two dyes, PB6 and TIP, with a D-$\pi$-A structure (Figure 1b), but different in the $\pi$ linkers, are used as the photosensitizers. The energy levels of NiO, dyes, and $Al_2O_3$ are taken from our previous work.[20,23] For $SnO_2$, the energy levels are taken from the literature,[29] which has used a similar method to prepare ALD $SnO_2$.

The detailed process of ALD of $SnO_2$ into mesoporous NiO films is shown in Figure S1. According to our previous work,[20] the good core–shell structure of NiO and ALD $TiO_2$ can show ultrafast hole and electron injection, which is beneficial for the dye regeneration. In order to have good penetration of $SnO_2$ into the mesoporous NiO film, an extended precursor exposure time was applied in this work (see details in the Experimental Section). The process of ALD of $Al_2O_3$ is similar to ALD of $SnO_2$.

In order to observe the morphology of the films and check the status of $SnO_2$ penetration, scanning electron microscopy (SEM) is used to characterize the morphology of different layers. The SEM image of the sputter-deposited NiO blocking layer film is shown in Figure 2a. One can see a very dense and uniform NiO film, which is beneficial to effectively block the unwanted contact between FTO and $SnO_2$, avoiding short circuit from the contact of the back-contact and FTO surface. Figure 2b displays the SEM image of the mesoporous NiO film that is helpful for loading more dyes. After 100 cycles of ALD of $SnO_2$ (about 16 nm) layers into the mesoporous NiO film, the morphology of the NiO/ALD $SnO_2$ film still remains porous from the SEM image in Figure 2c but becomes denser. In order to check if the ALD $SnO_2$ and $Al_2O_3$ have good penetration into the mesoporous NiO film, energy-dispersive X-ray spectroscopy (EDX) of the cross-section SEM image (Figure 2d) of FTO/NiO/$Al_2O_3$/$SnO_2$ has been carried out. The result shows a uniform distribution of $SnO_2$ in the mesoporous film, indicating good penetration of ALD $SnO_2$ into the NiO film. Due to the presence of Sn in the FTO substrate, Sn can be also observed in the part of FTO in Figure 2f. The uniform distribution of $Al_2O_3$ in the mesoporous NiO film indicates better penetration than that in our previous work,[20] likely due to longer exposure time in the process of ALD.

A more intimate contact between $SnO_2$ and NiO (near to dye) can not only promote charge separation but also increase charge recombination, while use of a thin $Al_2O_3$ layer can suppress such charge recombination. From our previous study,[20] a thin ALD $Al_2O_3$ layer between dye and NiO did not influence the hole injection and a thin ALD $Al_2O_3$ layer between NiO and ETM did not influence fast electron injection from the dye to ETM. In this work, we sensitized dye first and then used ALD $Al_2O_3$, so the electronic coupling between NiO and the dye should not be significantly changed. The satisfactory penetration of $SnO_2$ and $Al_2O_3$ into mesoporous NiO films is therefore expected to accelerate charge separation and suppress charge recombination, thereby benefitting photovoltaic parameters.

To evaluate the photovoltaic performance of the solid-state p-type DSSCs, two kinds of devices, with or without $Al_2O_3$ layers, were assembled. For the device of FTO/NiO/dyes/$SnO_2$/Al, the photocurrent density–photovoltage ($J$–$V$)


https://doi.org/10.1021/acsaem.2c01328
ACS Appl. Energy Mater. 2022, 5, 12022–12028

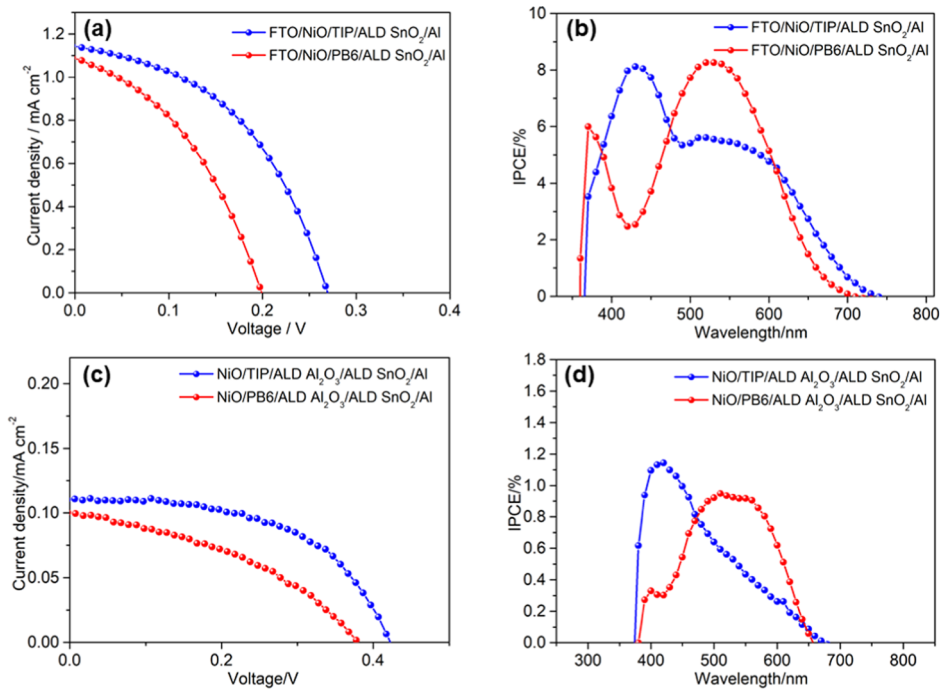


**Figure 3.** (a) Photocurrent density−photovoltage ($J$−$V$) curve and (b) IPCE spectra of FTO/NiO/PB6- and TIP/ALD $SnO_2$/Al-based devices and (c) photocurrent density−photovoltage ($J$−$V$) curve and (d) IPCE spectra of FTO/NiO/PB6- and TIP/ALD $Al_2O_3$/ALD $SnO_2$/Al-based devices (the thickness of $Al_2O_3$ and $SnO_2$ is 1 and 16 nm, respectively).

**Table 1. Photovoltaic Parameters of Solid-State p-Type DSSCs (Light Intensity: AM 1.5G, 100 mW $cm^{-2}$; Active Area: 0.125 $cm^{-2}$)**

| Device | $V_{oc}$ (V) | $J_{sc}$ (mA $cm^{-2}$) | FF | PCE (%) |
|---|---|---|---|---|
| FTO/NiO/PB6/$SnO_2$/Al | 0.199 | 1.082 | 0.397 | 0.086 |
| FTO/NiO/TIP/$SnO_2$/Al | 0.269 | 1.140 | 0.458 | 0.141 |
| FTO/NiO/PB6/$Al_2O_3$/$SnO_2$/Al | 0.381 | 0.100 | 0.392 | 0.015 |
| FTO/NiO/TIP/$Al_2O_3$/$SnO_2$/Al | 0.423 | 0.110 | 0.541 | 0.025 |

curves are shown in Figure 3a and their photovoltaic parameters are listed in Table 1. A PCE of 0.086% was achieved with a $V_{oc}$ of 0.199 V, a $J_{sc}$ of 1.082 mA $cm^{-2}$, and a FF of 0.397 when PB6 dye was used in the device. Using TIP dye instead of PB6 dye, the FTO/NiO/TIP/$SnO_2$/Al-based device reached a PCE of 0.141% with a $V_{oc}$ of 0.269 V, a $J_{sc}$ of 1.141 mA $cm^{-2}$, and a FF of 0.458. The $J_{sc}$ of the FTO/NiO/TIP/$SnO_2$/Al-based device is a record for the solid-state p-type DSSCs. When the dyes were varied in FTO/NiO/dyes/$SnO_2$/Al-based devices, the TIP dye-based device attained higher $V_{oc}$ and FF values than those of the PB6 dye-based device. Such results can be attributed to the $\pi$ bridge in TIP dye having a stronger ability to suppress the charge recombination between holes in the NiO VB and electrons in the $SnO_2$ CB in the solar cell than the PB6 dye does. The IPCE spectra of FTO/NiO/dyes/$SnO_2$/Al-based devices are shown in Figure 3b. The maximum value of IPCE is beyond 8%, which is a big progress for solid-state p-type DSSCs. Although the $J_{sc}$ values of FTO/NiO/dyes/$SnO_2$/Al-based devices are largely improved, the $V_{oc}$ of such devices is still lower than what we reported previously using other metal oxides as ETMs.[20,22] The positive CB of $SnO_2$ and unwanted charge recombination may contribute to the low $V_{oc}$. To suppress the charge recombination, an ALD $Al_2O_3$ layer with 10 cycles (about 1 nm) was deposited on the NiO/dyes film prior to ALD of $SnO_2$ to form the FTO/NiO/dyes/$Al_2O_3$/$SnO_2$/Al-based device. For the FTO/NiO/PB6/$Al_2O_3$/$SnO_2$/Al-based device (Figure 3c), a $V_{oc}$ of 0.381 V was reached, which is much higher than that of the FTO/NiO/PB6/$SnO_2$/Al-based ($V_{oc}$ = 0.199 V) device without $Al_2O_3$. A similar phenomenon can be observed for the TIP dye-based device, which achieved a $V_{oc}$ of 0.423 V with $Al_2O_3$ in the device. The theoretical photovoltage of the device based on $SnO_2$ ETM is 0.5 V determined from the potential difference between the VB of NiO and the CB of $SnO_2$. These results indicate that the ALD of $Al_2O_3$ can effectively suppress the charge recombination and therefore enhance the $V_{oc}$ of solid-state p-type DSSCs. In addition, the FF (0.541) of the TIP dye-based device is also enhanced. However, the $J_{sc}$ of the FTO/NiO/dyes/$Al_2O_3$/$SnO_2$/Al-based device is much lower than that of the device without $Al_2O_3$, and the maximum IPCE (Figure 3d) value of FTO/NiO/dyes/$Al_2O_3$/$SnO_2$/Al is reduced to about 1%. In our previous work,[20] we did not observe that the hole injection from the dye was significantly affected by introduction of a thick $Al_2O_3$ layer.

In our previous work, we found that the electron injection from the reduced dye to NiO surface states is an interface charge transfer pathway.[30] Considering the energy levels of NiO surface states (ca. +0.6 to −0.4 vs NHE) and $SnO_2$ CB (0 vs NHE), the electron transfer from the injected electrons in NiO surface states to the $SnO_2$ CB is also thermodynamically feasible. Therefore, besides direct electron injection from the


https://doi.org/10.1021/acsaem.2c01328
ACS Appl. Energy Mater. 2022, 5, 12022−12028

reduced dye to $SnO_2$, the electron injection via NiO surface states to $SnO_2$ could be another pathway. However, when one cycle of $Al_2O_3$ is applied to passivate the majority of the NiO surface states, the direct electron transfer from the reduced dye to $SnO_2$ should dominate the charge separation process. A mechanism scheme of interface charge separation is shown in Figure 4. In addition, the conductivity of the NiO film is

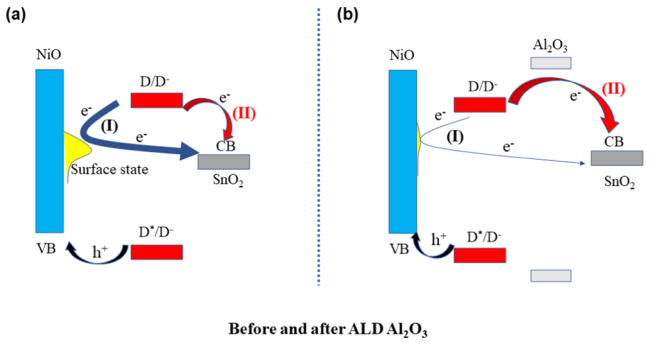


**Figure 4.** Possible process of electron transfer before and after ALD of $Al_2O_3$.

decreased obviously after inserting $Al_2O_3$,[30] which could have a negative effect on the $J_{sc}$ as well. The reduced $J_{sc}$ could be therefore explained by the removal of NiO surface states by $Al_2O_3$which influences interface charge transfer and the hole transport in NiO films.[30]

To elucidate the variation of $V_{oc}$ and $J_{sc}$ after ALD of $Al_2O_3$, transient photovoltage/photocurrent techniques are used to analyze the process of charge transport. The relation between charge lifetime and photovoltage is shown in Figure 5a. The $V_{oc}$ is adjusted with different light intensities. As shown in Figure 5a, the FTO/NiO/PB6/$Al_2O_3$/$SnO_2$/Al-based device has a much longer charge lifetime than that of the FTO/NiO/PB6/$SnO_2$/Al-based device, which suggests that inserting $Al_2O_3$ into the device can effectively suppress the charge recombination and then improve photovoltage of the device.[24,30] The same trend can be observed in Figure 5a for the TIP dye-based device. In addition, the charge lifetime of FTO/NiO/TIP/$Al_2O_3$/$SnO_2$/Al is longer than that of the FTO/NiO/PB6/$Al_2O_3$/$SnO_2$/Al-based device. These results indicate that the TIP dye with indacenodithieno[3,2-*b*]-thiophene as a $\pi$ linker has a stronger ability in suppressing the charge recombination than the PB6 dye with thiophene as a $\pi$ linker.[23] As a result, the TIP dye-based device can reach higher $V_{oc}$ than that of the PB6 dye-based device under the same condition (with or without $Al_2O_3$), which is consistent with previous reports.[23,31] To explain why the FTO/NiO/dyes/$SnO_2$/Al-based device has a much higher $J_{sc}$ than the FTO/NiO/dyes/$Al_2O_3$/$SnO_2$/Al-based device, the dependence of charge transport time on photocurrent is measured.[32,33] As displayed in Figure 5b, the FTO/NiO/dyes/$SnO_2$/Al-based device has a much shorter charge transport time than that of the FTO/NiO/PB6/$Al_2O_3$/$SnO_2$/Al-based device, which can explain the higher photocurrent density obtained from the devices without $Al_2O_3$ layers. After tracking the PCE of the FTO/NiO/PB6/$SnO_2$/Al-based device for above 1300 h under the air condition in dark, the device can maintain over 88% of the highest PCE (Figure S7).

To assess effects of thickness of the $Al_2O_3$ layer on the performance, three different thicknesses of the $Al_2O_3$ layer (0.1, 0.5, and 1 nm) were prepared. The *J*−*V* curve is shown in Figure 6 and the corresponding photovoltaic data are collected

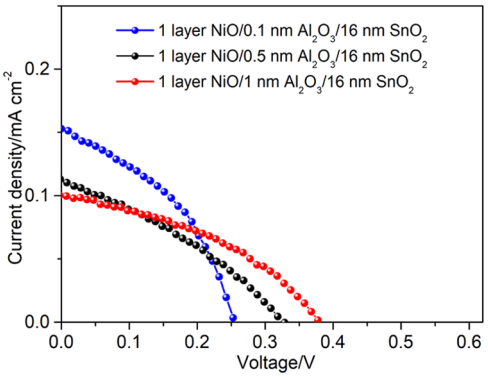


**Figure 6.** *J*−*V* curves of solid-state p-type DSSCs (FTO/NiO/PB6/$Al_2O_3$/$SnO_2$/Al) with different thicknesses of the $Al_2O_3$ layer.

in Table S3. In this paper, we used the ALD method we reported[30] previously to remove NiO surface states. As a result, a very obvious decrease in $J_{sc}$ is observed by inserting one cycle (0.1 nm) of $Al_2O_3$ because of NiO surface states, which has been suggested to be the one of hole transport channels in the previous studies.[34] With the increased thickness of the $Al_2O_3$ layer, the $J_{sc}$ is decreased by a low degree. In our previous work, we used transient absorption spectroscopy to measure the ultrafast regeneration of the NiO/dye/$Al_2O_3$/$TiO_2$-based system. We found that the introduction of one cycle of $Al_2O_3$ did not influence the fast electron injection from dye to the

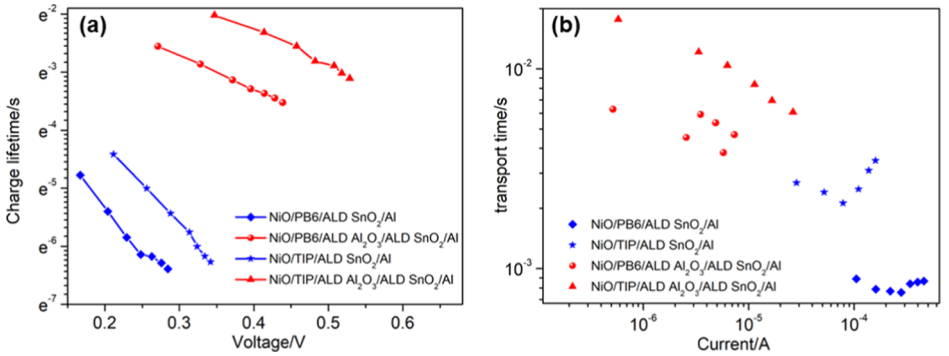


**Figure 5.** (a) Relation between charge lifetime and voltage for NiO/dye/$SnO_2$/Al- and NiO/dye/$Al_2O_3$/$SnO_2$/Al-based devices and (b) relation of charge transport time with current.



https://doi.org/10.1021/acsaem.2c01328
ACS Appl. Energy Mater. 2022, 5, 12022−12028

$TiO_2$ CB.[20,21] Therefore, in the NiO/dye/$Al_2O_3$/$SnO_2$-based system, the electron injection in the CB of $SnO_2$ should be also efficient enough. However, the $V_{oc}$ is improved with the increased thickness of $Al_2O_3$ due to suppression of charge recombination between the injected holes in NiO and injected electrons in $SnO_2$. The trend is different from our previous result when we used $TiO_2$ as ETM.[20] There could be two possibilities: (i) The ALD method we used previously in $TiO_2$ work did not completely remove the NiO surface states, which is evident from the charge transport time in our previous work,[20] where we observed that the charge transport time is constant and not dependent on light intensity. With the removal of NiO surface states, the charge transport time is dependent on light intensity as shown in Figure 5 in this work. The same trend can be also observed in our previous work with the similar ALD method.[30] (ii) In $SnO_2$-based devices, the injected electrons in NiO surface states by excited dye transfer to the $SnO_2$ CB play a crucial role in charge separation. Introduction of $Al_2O_3$ passivates the majority of NiO surface states and therefore significantly decreases $J_{sc}$. The decrease in NiO conductivity should be also responsible for the decreased $J_{sc}$. Also, according to our previous work,[30] the dye sensitization can protect some surface states from ALD $Al_2O_3$. When the thickness of $Al_2O_3$ is increased, the electron transfer from the protected NiO surface states to the $SnO_2$ CB will be slowed down, causing decreased $J_{sc}$. This is different from the $TiO_2$-based device, where the injected electrons in NiO surface sates cannot be efficiently used due to more negative potential of the $TiO_2$ CB than that of NiO surface states. Prasittichai and Hupp reported $SnO_2$/$Al_2O_3$ in liquid-electrolyte DSSCs[35] and used one cycle of ALD of $Al_2O_3$ to passivate the $SnO_2$-based photoanode, which improved the $V_{oc}$, FF, and electron lifetime very obviously. Their result is in consistence with our result in this work.

## CONCLUSIONS

In summary, $SnO_2$ ETM is prepared by the ALD method in a dye-sensitized mesoporous NiO film for solid-state p-type DSSCs. By extending the exposure time in the ALD process, good penetration of $SnO_2$ into the mesoporous NiO film can be realized, which in turn permits good contact formation with dye-sensitized NiO particles. As a result, a photocurrent density above 1 mA $cm^{-2}$ is achieved using the FTO/NiO/dyes/$SnO_2$/Al-based device, which is a record for the solid-state p-type DSSCs. The FTO/NiO/TIP/$SnO_2$/Al-based device can reach a PCE of 0.14%. In addition, introduction of $Al_2O_3$ into the device can largely reduce the charge recombination to enhance the $V_{oc}$. This work shows the potential to further improve the efficiency of solid-state p-type DSSCs by optimizing ETMs and dyes.

## ASSOCIATED CONTENT

### Supporting Information

The Supporting Information is available free of charge at https://pubs.acs.org/doi/10.1021/acsaem.2c01328.

Process of ALD; device structure; SEM; absorption of dye on NiO films; $J-V$ curves; stability of the device; and photovoltaic parameters of solid-state p-type DSSCs (PDF)

## AUTHOR INFORMATION


### Corresponding Author

**Haining Tian** − *Department of Chemistry-Ångström Laboratory, Physical Chemistry, Uppsala University, SE-751 20 Uppsala, Sweden;* orcid.org/0000-0001-6897-2808; Email: haining.tian@kemi.uu.se

### Authors

**Haoliang Cheng** − *Department of Chemistry-Ångström Laboratory, Physical Chemistry, Uppsala University, SE-751 20 Uppsala, Sweden;* orcid.org/0000-0002-3941-488X

**Yawen Liu** − *Department of Chemistry-Ångström Laboratory, Physical Chemistry, Uppsala University, SE-751 20 Uppsala, Sweden*

**Bin Cai** − *Department of Chemistry-Ångström Laboratory, Physical Chemistry, Uppsala University, SE-751 20 Uppsala, Sweden*

**Carl Hägglund** − *Division of Solar Cell Technology, Department of Materials Science and Engineering, Uppsala University, SE-75120 Uppsala, Sweden;* orcid.org/0000-0001-6589-3514

**Tomas Kubart** − *Department of Engineering Sciences, Uppsala University, SE-75120 Uppsala, Sweden*

**Gerrit Boschloo** − *Department of Chemistry-Ångström Laboratory, Physical Chemistry, Uppsala University, SE-751 20 Uppsala, Sweden;* orcid.org/0000-0002-8249-1469

Complete contact information is available at: https://pubs.acs.org/10.1021/acsaem.2c01328


### Notes

The authors declare no competing financial interest.

## ACKNOWLEDGMENTS

We gratefully thank the financial support from the Carl-Trygger Foundation (CT 19:370), Göran Gustafsson Foundation (nr 2029, 2127 and 2220), and the Wenner-Gren Foundation (UPD2021-0151). We also thank Dr. Bo Xu for providing the TIP dye.

## REFERENCES


(1) O'Regan, B.; Grätzel, M. A low-cost, high-efficiency solar cell based on dye-sensitized colloidal TiO2 films. *Nature* **1991**, *353*, 737−740.

(2) Hagfeldt, A.; Boschloo, G.; Sun, L.; Kloo, L.; Pettersson, H. Dye-Sensitized Solar Cells. *Chem. Rev.* **2010**, *110*, 6595−6663.

(3) Wang, Z.-S.; Kawauchi, H.; Kashima, T.; Arakawa, H. Significant influence of $TiO_2$ photoelectrode morphology on the energy conversion efficiency of N719 dye-sensitized solar cell. *Coord. Chem. Rev.* **2004**, *248*, 1381−1389.

(4) Hu, L.; Dai, S.; Weng, J.; Xiao, S.; Sui, Y.; Huang, Y.; Chen, S.; Kong, F.; Pan, X.; Liang, L.; Wang, K. Microstructure Design of Nanoporous $TiO_2$ Photoelectrodes for Dye-Sensitized Solar Cell Modules. *J. Phys. Chem. B* **2007**, *111*, 358−362.

(5) He, J.; Lindström, H.; Hagfeldt, A.; Lindquist, S.-E. Dye-Sensitized Nanostructured p-Type Nickel Oxide Film as a Photocathode for a Solar Cell. *J. Phys. Chem. B* **1999**, *103*, 8940−8943.

(6) Odobel, F.; Le Pleux, L.; Pellegrin, Y.; Blart, E. New Photovoltaic Devices Based on the Sensitization of p-type Semiconductors: Challenges and Opportunities. *Acc. Chem. Res.* **2010**, *43*, 1063−1071.

(7) Gibson, E. A.; Smeigh, A. L.; Le Pleux, L.; Fortage, J.; Boschloo, G.; Blart, E.; Pellegrin, Y.; Odobel, F.; Hagfeldt, A.; Hammarström, L. A p-Type NiO-Based Dye-Sensitized Solar Cell with an Open-Circuit Voltage of 0.35 V. *Angew. Chem., Int. Ed.* **2009**, *48*, 4402−4405.

(8) Xu, Z.; Xiong, D.; Wang, H.; Zhang, W.; Zeng, X.; Ming, L.; Chen, W.; Xu, X.; Cui, J.; Wang, M.; Powar, S.; Bach, U.; Cheng, Y.-B.

Remarkable photocurrent of p-type dye-sensitized solar cell achieved by size controlled $CuGaO_2$ nanoplates. *J. Mater. Chem. A* **2014**, *2*, 2968−2976.
(9) Tian, H.; Oscarsson, J.; Gabrielsson, E.; Eriksson, S. K.; Lindblad, R.; Xu, B.; Hao, Y.; Boschloo, G.; Johansson, E. M. J.; Gardner, J. M.; Hagfeldt, A.; Rensmo, H.; Sun, L. Enhancement of p-Type Dye-Sensitized Solar Cell Performance by Supramolecular Assembly of Electron Donor and Acceptor. *Sci. Rep.* **2014**, *4*, 4282.
(10) Perera, I. R.; Daeneke, T.; Makuta, S.; Yu, Z.; Tachibana, Y.; Mishra, A.; Bäuerle, P.; Ohlin, C. A.; Bach, U.; Spiccia, L. Application of the Tris(acetylacetonato)iron(III)/(II) Redox Couple in p-Type Dye-Sensitized Solar Cells. *Angew. Chem., Int. Ed.* **2015**, *54*, 3758−3762.
(11) Qin, P.; Zhu, H.; Edvinsson, T.; Boschloo, G.; Hagfeldt, A.; Sun, L. Design of an Organic Chromophore for P-Type Dye-Sensitized Solar Cells. *J. Am. Chem. Soc.* **2008**, *130*, 8570−8571.
(12) Wrede, S.; Tian, H. Towards sustainable and efficient p-type metal oxide semiconductor materials in dye-sensitised photocathodes for solar energy conversion. *Phys. Chem. Chem. Phys.* **2020**, *22*, 13850−13861.
(13) Li, F.; Fan, K.; Xu, B.; Gabrielsson, E.; Daniel, Q.; Li, L.; Sun, L. Organic Dye-Sensitized Tandem Photoelectrochemical Cell for Light Driven Total Water Splitting. *J. Am. Chem. Soc.* **2015**, *137*, 9153−9159.
(14) Dini, D.; Halpin, Y.; Vos, J. G.; Gibson, E. A. The influence of the preparation method of NiOx photocathodes on the efficiency of p-type dye-sensitized solar cells. *Coord. Chem. Rev.* **2015**, *304*−*305*, 179−201.
(15) Yu, M.; Natu, G.; Ji, Z.; Wu, Y. p-Type Dye-Sensitized Solar Cells Based on Delafossite $CuGaO_2$ Nanoplates with Saturation Photovoltages Exceeding 460 mV. *J. Phys. Chem. Lett.* **2012**, *3*, 1074−1078.
(16) D'Amario, L.; Antila, L. J.; Pettersson Rimgard, B.; Boschloo, G.; Hammarström, L. Kinetic Evidence of Two Pathways for Charge Recombination in NiO-Based Dye-Sensitized Solar Cells. *J. Phys. Chem. Lett.* **2015**, *6*, 779−783.
(17) D'Amario, L.; Jiang, R.; Cappel, U. B.; Gibson, E. A.; Boschloo, G.; Rensmo, H.; Sun, L.; Hammarström, L.; Tian, H. Chemical and Physical Reduction of High Valence Ni States in Mesoporous NiO Film for Solar Cell Application. *ACS Appl. Mater. Interfaces* **2017**, *9*, 33470−33477.
(18) Zhang, L.; Boschloo, G.; Hammarström, L.; Tian, H. Solid state p-type dye-sensitized solar cells: concept, experiment and mechanism. *Phys. Chem. Chem. Phys.* **2016**, *18*, 5080−5085.
(19) Pham, T. T. T.; Saha, S. K.; Provost, D.; Farré, Y.; Raissi, M.; Pellegrin, Y.; Blart, E.; Vedraine, S.; Ratier, B.; Aldakov, D.; Odobel, F.; Bouclé, J. Toward Efficient Solid-State p-Type Dye-Sensitized Solar Cells: The Dye Matters. *J. Phys. Chem. C* **2017**, *121*, 129−139.
(20) Tian, L.; Föhlinger, J.; Zhang, Z.; Pati, P. B.; Lin, J.; Kubart, T.; Hua, Y.; Sun, J.; Kloo, L.; Boschloo, G.; Hammarström, L.; Tian, H. Solid state p-type dye sensitized NiO−dye−$TiO_2$ core−shell solar cells. *Chem. Commun.* **2018**, *54*, 3739−3742.
(21) Tian, L.; Föhlinger, J.; Pati, P. B.; Zhang, Z.; Lin, J.; Yang, W.; Johansson, M.; Kubart, T.; Sun, J.; Boschloo, G.; Hammarström, L.; Tian, H. Ultrafast dye regeneration in a core−shell NiO−dye−TiO2 mesoporous film. *Phys. Chem. Chem. Phys.* **2018**, *20*, 36−40.
(22) Xu, B.; Tian, L.; Etman, A. S.; Sun, J.; Tian, H. Solution-processed nanoporous NiO-dye-ZnO photocathodes: Toward efficient and stable solid-state p-type dye-sensitized solar cells and dye-sensitized photoelectrosynthesis cells. *Nano Energy* **2019**, *55*, 59−64.
(23) Xu, B.; Wrede, S.; Curtze, A.; Tian, L.; Pati, P. B.; Kloo, L.; Wu, Y.; Tian, H. An Indacenodithieno[3,2-b]thiophene-Based Organic Dye for Solid-State p-Type Dye-Sensitized Solar Cells. *ChemSusChem* **2019**, *12*, 3243−3248.
(24) Tian, L.; Törndahl, T.; Lin, J.; Pati, P. B.; Zhang, Z.; Kubart, T.; Hao, Y.; Sun, J.; Boschloo, G.; Tian, H. Mechanistic Insights into Solid-State p-Type Dye-Sensitized Solar Cells. *J. Phys. Chem. C* **2019**, *123*, 26151−26160.
(25) Tian, H. Solid-state p-type dye-sensitized solar cells: progress, potential applications and challenges. *Sustainable Energy Fuels* **2019**, *3*, 888−898.
(26) Jiang, Q.; Zhang, X.; You, J. $SnO_2$: A Wonderful Electron Transport Layer for Perovskite Solar Cells. *Small* **2018**, *14*, 1801154.
(27) Min, H.; Lee, D. Y.; Kim, J.; Kim, G.; Lee, K. S.; Kim, J.; Paik, M. J.; Kim, Y. K.; Kim, K. S.; Kim, M. G.; Shin, T. J.; Il Seok, S. Perovskite solar cells with atomically coherent interlayers on $SnO_2$ electrodes. *Nature* **2021**, *598*, 444−450.
(28) Snaith, H. J.; Ducati, C. $SnO_2$-Based Dye-Sensitized Hybrid Solar Cells Exhibiting Near Unity Absorbed Photon-to-Electron Conversion Efficiency. *Nano Lett.* **2010**, *10*, 1259−1265.
(29) Baena, J. P. C.; Steier, L.; Tress, W.; Saliba, M.; Neutzner, S.; Matsui, T.; Giordano, F.; Jacobsson, T. J.; Kandada, A. R. S.; Zakeeruddin, S. M.; Petrozza, A. Highly Efficient Planar Perovskite Solar Cells Through Band Alignment Engineering. *Energy Environ. Sci.* **2015**, *8*, 2928−2934.
(30) Tian, L.; Tyburski, R.; Wen, C.; Sun, R.; Abdellah, M.; Huang, J.; D'Amario, L.; Boschloo, G.; Hammarström, L.; Tian, H. Understanding the Role of Surface States on Mesoporous NiO Films. *J. Am. Chem. Soc.* **2020**, *142*, 18668−18678.
(31) Ji, Z.; Natu, G.; Huang, Z.; Wu, Y. Linker effect in organic donor−acceptor dyes for p-type NiO dye sensitized solar cells. *Energy Environ. Sci.* **2011**, *4*, 2818−2821.
(32) Anta, J. A.; Casanueva, F.; Oskam, G. A Numerical Model for Charge Transport and Recombination in Dye-Sensitized Solar Cells. *J. Phys. Chem. B* **2006**, *110*, 5372−5378.
(33) Martinson, A. B. F.; McGarrah, J. E.; Parpia, M. O. K.; Hupp, J. T. Dynamics of charge transport and recombination in ZnO nanorod array dye-sensitized solar cells. *Phys. Chem. Chem. Phys.* **2006**, *8*, 4655−4659.
(34) Zhu, H.; Hagfeldt, A.; Boschloo, G. Photoelectrochemistry of Mesoporous NiO Electrodes in Iodide/Triiodide Electrolytes. *J. Phys. Chem. C* **2007**, *111*, 17455−17458.
(35) Prasittichai, C.; Hupp, J. T. Surface Modification of $SnO_2$ Photoelectrodes in Dye-Sensitized Solar Cells: Significant Improvements in Photovoltage via $Al_2O_3$ Atomic Layer Deposition. *J. Phys. Chem. Lett.* **2010**, *1*, 1611−1615.


https://doi.org/10.1021/acsaem.2c01328
*ACS Appl. Energy Mater.* 2022, 5, 12022−12028